HHS Public Access

Author manuscript

Invest Radiol. Author manuscript; available in PMC 2018 November 01.

Published in final edited form as:

Invest Radiol. 2017 November ; 52(11): 686–692. doi:10.1097/RLI.0000000000000390.

Magnetization Transfer MRI Noninvasively Detects Renal Fibrosis in Swine Atherosclerotic Renal Artery Stenosis at 3.0 T

Kai Jiang, PhD[1], **Christopher M. Ferguson, MS**[1], **John R. Woollard, MS**[1], **Xiangyang Zhu, MD, PhD**[1], and **Lilach O. Lerman, MD, PhD**[1]

[1]Division of Nephrology and Hypertension, Mayo Clinic, Rochester, Minnesota, USA

Abstract

Objectives—Renal fibrosis is a useful biomarker for diagnosis and evaluation of therapeutic interventions of renal diseases, but often requires invasive testing. Magnetization transfer magnetic resonance imaging (MT-MRI), which evaluates the presence of macromolecules, offers a noninvasive tool to probe renal fibrosis in murine renal artery stenosis (RAS) at 16.4T. In this study, we aimed to identify appropriate imaging parameters for collagen detection at 3.0T MRI and to test the utility of MT-MRI in measuring renal fibrosis in a swine model of atherosclerotic RAS (ARAS).

Materials and Methods—To select the appropriate offset frequency, an MT-MRI study was performed on a phantom containing 0–40% collagen I&III with offset frequencies from -1600 to +1600Hz and other MT parameters empirically set as pulse width 16ms and flip angle 800°. Then selected MT parameters were used *in vivo* on pigs 12 weeks after sham (n=8) or RAS (n=10) surgeries. The ARAS pigs were fed with high-cholesterol diet to induce atherosclerosis. The MT ratio (MTR) was compared to *ex-vivo* renal fibrosis measured using Sirius-red staining.

Results—Offset frequencies at 600 and 1000Hz were selected for collagen detection without direct saturation of free water signal, and subsequently applied *in vivo*. The ARAS kidneys showed mild cortical and medullary fibrosis by Sirius-red staining. The cortical and medullary MTRs at 600 and 1000Hz were both increased. Renal fibrosis measured *ex vivo* showed good linear correlations with MTR at 600 (cortex: Pearson's correlation coefficient r=0.87, P<0.001; medulla: r=0.70, P=0.001) and 1000Hz (cortex: r=0.75, P<0.001; medulla: r=0.83, P<0.001).

Conclusions—MT-MRI can noninvasively detect renal fibrosis in the stenotic swine kidney at 3.0T. Therefore, MT-MRI may potentially be clinically applicable and useful for detection and monitoring of renal pathology in subjects with RAS.

Keywords

Atherosclerotic renal artery stenosis; renal fibrosis; collagen; magnetization transfer magnetic resonance imaging; kidney segmentation

*Address correspondence to: Lilach O. Lerman, MD, Ph.D., Division of Nephrology and Hypertension, Mayo Clinic, 200 First St SW, Rochester, MN 55905, Tel: (507)266-9376 Fax: (507)266-9316, Lerman.Lilach@mayo.edu.

DISCLOSURES of CONFLICTS of INTEREST

None.

INTRODUCTION

Renal artery stenosis (RAS), a vascular disorder that induces kidney ischemia and remodeling, may ultimately lead to end stage-renal renal failure. In patients, atherosclerotic RAS (ARAS) accounts for approximately 90% of cases of RAS (1). ARAS is increasingly common in aging populations, particularly elderly people presenting with cardiovascular risk factors (2). Renal injury is exacerbated by atherosclerosis due to the concurrent atherogenic factors. The affected kidneys typically undergo progressive deposition and accumulation of extracellular matrix (ECM) components, composed mainly of fibronectin and collagen type I, III, and IV, that may evolve into tubulointerstitial fibrosis (3).

Renal fibrosis is a useful biomarker for diagnosis and evaluation of therapeutic interventions of renal diseases, but its assessment often requires invasive methods such as tissue biopsy. Notably, invasive methods are also prone to sampling error and observer variability, and may result in complications (4). Recently, noninvasive MR-based imaging techniques, such as diffusion-weighted MRI (5–9) and magnetic resonance elastography (10, 11), have been implemented to detect renal fibrosis. Although these methods have been shown to be effective, susceptibility to structural and hemodynamic changes other than renal fibrosis hampers their specificity for measuring fibrosis. Therefore, a noninvasive method that is specific for fibrosis is needed to afford early diagnosis and gauge progression of renal injury, as well as monitor success of therapeutic approaches.

Magnetization transfer imaging (MTI) can evaluate the amount of macromolecules in tissue based on interactions of protons from the free water and macromolecule pools (12, 13). Selective saturation of the macromolecule pool leads to a signal decrease of the free water pool as a result of cross relaxation or chemical exchange between these two pools. Compared to conventional T_1-, T_2-, or proton density-weighted MRI techniques, MTI is more specific for evaluation of macromolecules. It has been applied to detect microstructural disruptions in the brain (14, 15), tissue composition in diseased lungs (16) and kidneys (17), and fibrosis in intestines (18–20), rectal cancer (21) and mouse kidneys (22).

MT parameters for collagen detection in murine RAS at 16.4T were recently identified, and the applicability of MT-MRI in measuring and monitoring longitudinal progression of renal fibrosis demonstrated (23). However, its capability for detecting renal fibrosis at clinical field-strength remains unknown. A novel swine model of unilateral ARAS also closely mimics human pathophysiology (24, 25). Compared to mice, the pig represents a favorable model to study renal disease as its anatomy, physiology, and pathophysiology are comparable to humans' (26).

In this study, we tested the hypothesis that MT-MRI would provide reliable assessments of renal cortical and medullary fibrosis in swine with unilateral ARAS at 3.0T. We initially determined the appropriate offset frequencies for collagen detection using a phantom study. In addition, due to multiple renal medullary pyramids, manual selection of region of interest (ROI) in pig kidneys is laborious and time-consuming. Therefore, we developed an algorithm for semi-automatic kidney segmentation during data analysis. We hypothesized

that *in vivo* MT would correlate with *ex vivo* measurement of renal fibrosis determined by histology in both the cortex and medulla.

MATERIALS AND METHODS

Phantom Study

MRI studies were performed on a GE Signa HDxt 3.0T scanner using an MT-prepared gradient echo sequence. To select the appropriate offset frequency, an MT-MRI study was initially performed on a phantom containing collagen types I and III (NeoCell, Newport Beach, CA) at 40%, 30%, 20%, 10% and 0% concentrations in pure water (Fig. 1). Images without MT preparation (M_o) were first acquired with the following parameters: TR 300ms; TE 3.4ms; flip angle 30°; slice thickness 4mm; slice number 5; FOV 15×15cm^2; matrix size 128×128; number of averages 1. Then MT-weighed images (M_t) were acquired by adding Fermi pulses prior to image acquisition with offset frequencies from -1600 to +1600Hz with an increment step of 200Hz. Other MT parameters were empirically set as pulse width 16ms, flip angle 800°, and one pulse per repetition.

Animals

This study was approved by the Institutional Animal Care and Use Committee. Domestic female control pigs (n=8) underwent a sham procedure and then fed with standard diet for 12 weeks. Unilateral RAS was induced in 10 other pigs by implantation in the right renal artery of a balloon-expandable local irritant coil under fluoroscopy, a model that we developed (27). These pigs were also fed with a standard 2% high-cholesterol diet (28, 29), including 15% Lard (Harlan Teklad, Madison, WI), starting from 6 weeks prior to surgery to induce early atherosclerosis (ARAS) and thereby aggravate fibrosis. All animals had free access to water.

In Vivo MT Study

The MT study was performed 12 weeks after surgery using the same sequence as in the phantom study. Anesthesia was induced with intramuscular injection of 5mg/kg Telazol (Zoetis Inc., Kalamazoo, MI) and 2mg/kg xylazine (Xylamed BiMeda Inc., Cambridge, ON, Canada), and maintained with 1–2% isoflurane. The pigs were also intubated for respiratory control. Coronal images of the kidney were acquired with the following imaging parameters as determined in the phantom study: offset frequency 600 and 1000Hz; slice thickness 2.6mm; slice number 5; FOV 35×35cm^2; matrix size 192×128, phase field-of-view 0.75; reconstruction matrix size 256×256. All other imaging parameters were the same as in the phantom study.

For selection of cortical and medullary ROIs, T_1/T_2^*-weighted images were acquired using a multi-echo gradient echo sequence with the same anatomical prescription as in the MT study. Multiple images with a repetition time of 200ms and echo times from 16 to 40ms were acquired and the one with the highest signal-to-noise ratio and cortical-medullary distinction was selected for kidney segmentation. To avoid respiratory motion, all MRI scans were performed with suspended respiration.

In Vivo MDCT Study

Single-kidney hemodynamics and function were assessed using multiple detector computed tomography (MDCT) two days after MRI. Animals were anesthetized as in the MRI study, and anesthesia was maintained with intravenous infusion of ketamine (0.2mg/kg per minute, Hospria Inc., Lake Forest, IL) and xylazine (0.03mg/kg per minute) throughout the course of imaging. The degree of RAS was assessed using selective angiography. A blood sample was collected from the inferior vena cava, and mean arterial pressure measured using a carotid artery catheter. For renal perfusion and glomerular filtration rate (GFR), 140 consecutive scans were continuously acquired in 3 contiguous 5-mm slices following a bolus injection of iopamidol (0.5mL/kg in 2 seconds, Omnipaque®, Novalplus, USA) through a catheter placed in the right atrium (30). Renal volume was measured 15 min after the flow study to allow contrast washout. Another bolus of iopamidol (0.5mL/kg over 5 sec) was injected and 30–34 contiguous 5mm-thick slices covering the whole kidney were imaged.

Image Analysis

All MRI images were analyzed using software modules developed in-house in Matlab (Mathworks, Natick, MA). The magnetization transfer ratio (MTR) map was calculated in both kidneys pixel-wise as $(M_0-M_t)/M_0$. Renal MTR was normalized by dorsal muscle MTR to correct for intra- and inter-subject B_1 inhomogeneity. Due to the moderate contrast in MT images (Fig. 2a–b), cortical and medullary ROIs were selected on T_1/T_2^*-weighted anatomical images of the same slices (Fig. 2e). A larger T_1 in renal medulla leads to lower signal intensity in T_1-weighed image (31), whereas lower oxygenation makes the medulla appear darker than the cortex in T_2^*-weighted images (32). Therefore, a combination of T_1 and T_2^* weighting gives rise to a good cortical-medullary contrast. A Matlab-based module was implemented for semi-automatic selection of cortical and medullary ROIs following several steps (Fig. 2f): 1). Exclusion of the collecting system; 2). Image segmentation by thresholding (33); 3). Image opening to correct misclassified pixels in renal cortex; 4). Edge detection of the borders of cortex and medulla. The threshold for image segmentation and the kernel size for image opening were manually edited to adjust ROI selection. The proposed algorithm provided a visually satisfactory segmentation of cortex and medulla (Fig. 2g). The selected ROIs were then propagated and applied for quantification of cortical and medullary MTRs. Mean values from all ROIs in different slices were averaged.

MDCT images were analyzed using the Analyze™ software package (Biomedical Imaging Resource, Mayo Clinic, Rochester, MN). Kidney volume was quantified based on the cortical and medullary ROIs manually placed on all frames where kidney was observed. For renal hemodynamics and function, tissue attenuation curves were generated from aorta, renal cortex, and medulla, and fitted by an in-house developed Matlab module to quantify renal perfusion and normalized GFR (34, 35). Renal blood flow (RBF) was calculated as the sum of the products of cortical and medullary perfusions and corresponding volumes, and GFR (ml/min) by multiplying cortical volume (cc) and normalized GFR (ml/min/cc).

Ex Vivo Studies

All pigs were euthanized 3–5 days after the MDCT study, and kidneys harvested, fixed in 10% formalin, and processed for histology. Sirius-red staining was performed on 5-μm axial

slices of tissue corresponding to MR tomographic slices as per anatomic landmarks (36). Fibrosis was quantified as the fraction of fibrotic area over the total cross sectional area of the tissue using AxioVision4.8 (Carl Zeiss SMT, Oberkochen, Germany). Serum creatinine level was measured by using the DetectX Creatinine Detection kit (K002-^{1}H; Arbor Assays, Ann Arbor, Mich).

Statistical Analysis

Statistical analysis was performed using JMP 10.0 (SAS Institute, Cary, NC). Normality of the data was assessed using the Shapiro-Wilk test. Results were expressed as means ± standard deviations for normally distributed data, or medians with ranges in parentheses for non-normally distributed data. One-way analysis of variance followed by unpaired Student's t-test or the Wilcoxon rank-sum test was performed to compare the control and ARAS groups, as appropriate. The Pearson's correlation was used to compare fibrosis measured *in vivo* and *ex vivo*. A p value ≤0.05 was considered statistically significant.

RESULTS

Collagen Phantom Study

Representative MTR maps of the collagen phantom at 400, 600, 800, and 1000Hz offset frequencies are shown in Fig. 1a. Increasing collagen concentrations enhanced the MT effect and thereby gave rise to larger MTR. The MTRs obtained at different offset frequencies are shown in Fig. 1b. A smaller offset frequency resulted in a larger MTR, but also induced stronger direct saturation of free water signal. Overall, an offset frequency between 600 and 1000Hz was found to offer relatively high MT sensitivity with minimal direct saturation of the free water pool.

A good linear correlation was observed between collagen concentration and MTRs at 600 (R^2=0.979, Fig. 1c) and 1000Hz (R^2=0.935, Fig. 1d), indicating that MTRs at both offset frequencies can be used to index collagen concentration. Therefore, to achieve high MT sensitivity with little free water saturation, offset frequencies at 600 and 1000Hz were chosen for *in vivo* studies. Other MT parameters were kept the same as in the phantom study, i.e., pulse width at 16 ms, flip angle at 800°, and one pulse per repetition.

Animal Characteristics and Renal Function

The animal characteristics and renal functional indices are shown in Table 1. ARAS pigs had a moderate unilateral stenosis with a median of 72.5% (30–98%), with greater body weight (likely as a result of high-cholesterol diet), and mean arterial pressure (MAP).

ARAS induced a slight loss in renal function, as indicated by the elevated serum creatinine level. A significant decrease in both cortical and medullary volumes was observed in the ARAS kidneys, which was accompanied by impaired cortical perfusion. Consequently, RBF and GFR both decreased significantly in the stenotic kidneys, indicating the functional significance of the stenosis.

In Vivo MT

Shown in Fig. 2a–d are the representative M_0, M_t and the calculated MTR maps of a pair of control kidneys at the offset frequency of 600Hz. In most normal pigs, the mean cortical MTR in the right kidney was slightly larger than that of the left kidney at both 600 and 1000Hz, possibly because of B_1 field inhomogeneity. Indeed, slightly larger MTR was also observed in the right psoas muscle (Fig. 2c). In order to correct for the B_1 variation, the kidney MTR was normalized by MTR of ipsilateral psoas muscle, resulting in uniform looking normal kidneys (Fig. 2d). Similar to the phantom study, we observed an obvious disturbance on the free water signal at 400Hz, but not at 600–1000Hz (Supplemental Fig. 1).

Renal Fibrosis

Representative Sirius red stained tissue sections viewed under polarized light are shown in Fig. 3a. The stenotic ARAS kidneys showed greater fibrosis than controls in both the cortex (Fig. 3b, 7.4±2.1% vs. 4.0±0.9%, P=0.001) and medulla (Fig. 3b, 10.1±2.0% vs. 6.3±1.0%, P<0.001).

Representative MTR maps of the control and ARAS kidneys at 1000 and 600Hz are shown in Fig. 3c. Compared to control kidneys, the cortical (76.0±3.3% vs. 71.5±2.3%, P=0.005) and medullary (66.8±3.5% vs. 60.1±1.9%, P<0.001) MTRs in the stenotic ARAS kidneys at 1000Hz were increased by 6.3% and 11.1%, respectively (Fig. 3d). At 600Hz, a 4.3% increase in cortical (79.5±2.7% vs. 76.2±1.1%, P=0.006) and 7.2% in medullary (73.0±2.6% vs. 68.1±2.8%, P=0.001) MTR were also observed (Fig. 3d). Therefore, although MTRs at 600 and 1000Hz both showed significant increases, the latter better differentiated normal and stenotic ARAS kidneys. In the contralateral ARAS kidneys, cortical (1000Hz: 70.7±2.4%, P=0.001; 600Hz: 74.3±1.9%, P<0.001) and medullary (1000Hz: 60.3±2.9%, P=0.001; 600Hz: 67.0±2.8%, P<0.001) MTRs were also significantly lower than in the stenotic kidneys (Supplemental Fig. 2).

In addition, the ARAS pigs were sub-divided into two groups: moderate (stenosis≥75%, n=5) and severe (stenosis<75%, n=5) RAS (Supplemental Fig. 3a). Whereas moderate ARAS only induced slight increases in MTR, kidneys with severe stenosis showed 10.2% (78.8±1.3% vs. 71.5±2.3%, P<0.001) and 13.5% (68.3±2.8% vs. 60.1±1.9%, P<0.001) increases in cortical and medullary MTR at 1000Hz. At 600Hz, cortical and medullary MTRs showed smaller increases of 7.0% (81.6±1.5% vs. 76.3±1.1%, P<0.001) and 9.5% (74.6±1.1% vs. 68.1±2.9%, P=0.001), respectively (Supplemental Fig. 3b). Furthermore, only 1000Hz detected an increase in medullary fibrosis in moderate ARAS compared to normal kidneys. Cortical fibrosis quantified from Sirius-red-stained tissue sections showed strong correlations with MTRs at both 600 (Fig. 4a, Pearson's correlation coefficient r=0.87, P<0.001) and 1000Hz (Fig. 4c, r=0.75, P<0.001). In the renal medulla, *ex vivo* fibrosis also significantly associated with MTR at 600Hz (Fig. 4b, r=0.70, P=0.001) and 1000Hz (Fig. 4d, r=0.83, P<0.001).

DISCUSSION

This study demonstrates the capability of MTI in assessing fibrosis in swine stenotic ARAS kidneys. Appropriate MT parameters were selected in the collagen phantom, and applied in the *in vivo* MTI. The measured cortical and medullary MTRs both showed a good correlation with fibrosis measured *ex vivo* using Sirius red staining. Taken together, MTI might provide useful noninvasive indices of renal fibrosis.

Appropriate irradiation-offset frequencies need to be selected in order to optimize MTI. The MT module typically consists of multiple pulses with large flip angles, which may cause high specific absorption rate and thermal heating in biological tissue, if not properly controlled (37). With a high offset-frequency, a larger flip angle is required to maintain MT contrast-to-noise ratio, but when too low, direct saturation of free water signal causes imaging artifacts. Previously, an optimal offset frequency at 1500Hz has been identified for collagen detection at 16.4T (23). Given the field dependence of the optimal offset frequency, a collagen phantom study was first performed in this study at 3.0T. We found that offset-frequencies between 600 and 1000Hz provided high collagen saturation with negligible perturbation on free water signal with the pulse width and flip angle empirically set at 16ms and 800°, respectively.

Factors such as imperfect RF transmit coils may cause B_1 field inhomogeneity in MRI, i.e., spatial variation in the flip angle (38, 39). Differences in body size may also induce variations in B_1 field across subjects, which in turn might affect the degree of MT saturation, resulting in inaccurate MTRs. In our study, we observed both intra- and inter-subject variations in MTRs of both kidneys and psoas muscles. Therefore, in order to correct B_1 field inhomogeneity and ensure the reliability of MTI *in vivo*, we implemented normalization of the renal MTR by MTR of the ipsilateral psoas muscle.

ARAS compromised renal function, as evidenced by the increased MAP and serum creatinine, as well as the decreased stenotic kidney volume and hemodynamics. While we observed a wide range of stenosis severities, the median degree was moderate, and thus accompanied by development of an overall mild tubulointerstitial fibrosis in the affected kidneys. Therefore, this swine ARAS model provided a good opportunity for investigation of the capability of MTI in assessing a spectrum of fibrosis grades, including subtle increases in renal fibrosis. Indeed, we found a good correlation between *in vivo* MTR (at 600 and 1000Hz) and *ex vivo* renal fibrosis by Sirius red staining, suggesting that MTI provides reliable measurements of renal fibrosis in swine kidneys. The pig model recapitulates distinct features of human ARAS, evidenced by reduced renal oxygenation, excessive release of inflammatory cytokines, and infiltration of inflammatory cells (40–46). Therefore, MTI might potentially be useful to detect renal fibrosis in patients as well. A sizable number of patients with mild and moderate chronic kidney disease have mild (5–25%) renal fibrosis (47), implying that this tool may be clinically useful. The wide availability of the imaging sequence in clinical scanners and short acquisition time (~1.5 min for one M_0 and two M_t scans) also makes the MTI clinically applicable. In order to shorten the breath-hold period in patients, fast imaging techniques, such as generalized

autocalibrating partial parallel acquisition, sensitivity encoding, and non-Cartesian k-space sampling can be applied in the clinical setting to expedite data acquisition.

There are several limitations to our study. First, factors in the ARAS kidneys other than fibrosis, such as reduced renal perfusion, accumulation of other extracellular proteins, and inflammatory cell infiltration, might possibly affect MTR, and further studies are needed to investigate their influence on MTI. Second, MTRs at 1000Hz showed a larger difference between ARAS and normal kidneys than those at 600Hz. This might be induced by slight direct water saturation at 600Hz, due to a larger frequency spread of the free water as a result of in vivo susceptibility variation. Third, the ARAS pigs showed a wide range of RAS as a result of different biological responses to the irritating coils. Nevertheless, this variability provided the opportunity to test the applicability of MTI in detecting a range of swine renal fibrosis by comparing to histology. A better control of RAS can be achieved by direct reduction of the vessel diameter using an inflatable cuff (48). Fourth, the proposed semi-automatic segmentation method may not be applicable to kidneys with reduced cortico-medullary contrast as a result of chronic diseases, in which case manual segmentation may be warranted. In addition, we investigated the utility of MTI in detecting renal fibrosis only at 12 weeks after induction of RAS, and its ability to monitor progression or regression of renal fibrosis needs to be explored in future studies.

In conclusion, noninvasive MTI successfully measured mild renal tubulointerstitial fibrosis in swine kidneys with unilateral ARAS. MTR measurement in ROIs defined using a semi-automatic algorithm for kidney segmentation correlates well with *ex vivo* renal fibrosis. Therefore, MTI may be valuable for noninvasive assessment of renal pathology, and potentially for evaluation of the success of therapeutic interventions in patients with RAS.

Supplementary Material

Refer to Web version on PubMed Central for supplementary material.

Acknowledgments

Funding: This study was partly supported by National Institutes of Health Grants DK104273, DK102325, DK73608, HL123160, and C06-RR018898.

References

1. Safian RD, Textor SC. Renal-artery stenosis. N Engl J Med. 2001; 344(6):431–42. [PubMed: 11172181]
2. Balk E, Raman G, Chung M, et al. Effectiveness of management strategies for renal artery stenosis: a systematic review. Ann Intern Med. 2006; 145(12):901–12. [PubMed: 17062633]
3. Conway B, Hughes J. Cellular orchestrators of renal fibrosis. Qjm. 2012; 105(7):611–5. [PubMed: 22139500]
4. Hogan JJ, Mocanu M, Berns JS. The Native Kidney Biopsy: Update and Evidence for Best Practice. Clin J Am Soc Nephrol. 2016; 11(2):354–62. [PubMed: 26339068]
5. Ebrahimi B, Rihal N, Woollard JR, et al. Assessment of renal artery stenosis using intravoxel incoherent motion diffusion-weighted magnetic resonance imaging analysis. Invest Radiol. 2014; 49(10):640–6. [PubMed: 24743589]

6. Eisenberger U, Binser T, Thoeny HC, et al. Living renal allograft transplantation: diffusion-weighted MR imaging in longitudinal follow-up of the donated and the remaining kidney. Radiology. 2014; 270(3):800–8. [PubMed: 24475796]
7. Ebrahimi B, Textor SC, Lerman LO. Renal relevant radiology: renal functional magnetic resonance imaging. Clin J Am Soc Nephrol. 2014; 9(2):395–405. [PubMed: 24370767]
8. Hueper K, Khalifa AA, Brasen JH, et al. Diffusion-Weighted imaging and diffusion tensor imaging detect delayed graft function and correlate with allograft fibrosis in patients early after kidney transplantation. J Magn Reson Imaging. 2016; 44(1):112–21. [PubMed: 26778459]
9. Hennedige T, Koh TS, Hartono S, et al. Intravoxel incoherent imaging of renal fibrosis induced in a murine model of unilateral ureteral obstruction. Magn Reson Imaging. 2015; 33(10):1324–8. [PubMed: 26248270]
10. Warner L, Yin M, Glaser KJ, et al. Noninvasive In vivo assessment of renal tissue elasticity during graded renal ischemia using MR elastography. Invest Radiol. 2011; 46(8):509–14. [PubMed: 21467945]
11. Korsmo MJ, Ebrahimi B, Eirin A, et al. Magnetic resonance elastography noninvasively detects in vivo renal medullary fibrosis secondary to swine renal artery stenosis. Invest Radiol. 2013; 48(2): 61–8. [PubMed: 23262789]
12. Wolff SD, Balaban RS. Magnetization transfer imaging: practical aspects and clinical applications. Radiology. 1994; 192(3):593–9. [PubMed: 8058919]
13. Henkelman RM, Stanisz GJ, Graham SJ. Magnetization transfer in MRI: a review. NMR Biomed. 2001; 14(2):57–64. [PubMed: 11320533]
14. Dousset V, Grossman RI, Ramer KN, et al. Experimental allergic encephalomyelitis and multiple sclerosis: lesion characterization with magnetization transfer imaging. Radiology. 1992; 182(2): 483–91. [PubMed: 1732968]
15. Ge Y, Grossman RI, Udupa JK, et al. Magnetization transfer ratio histogram analysis of gray matter in relapsing-remitting multiple sclerosis. AJNR Am J Neuroradiol. 2001; 22(3):470–5. [PubMed: 11237968]
16. Kuzo RS, Kormano MJ, Lipton MJ. Magnetization transfer magnetic resonance imaging of parenchymal lung disease. Invest Radiol. 1995; 30(2):118–22. [PubMed: 7782187]
17. Wang F, Jiang R, Takahashi K, et al. Longitudinal assessment of mouse renal injury using high-resolution anatomic and magnetization transfer MR imaging. Magn Reson Imaging. 2014; 32(9): 1125–32. [PubMed: 25093632]
18. Adler J, Swanson SD, Schmiedlin-Ren P, et al. Magnetization transfer helps detect intestinal fibrosis in an animal model of Crohn disease. Radiology. 2011; 259(1):127–35. [PubMed: 21324841]
19. Pazahr S, Blume I, Frei P, et al. Magnetization transfer for the assessment of bowel fibrosis in patients with Crohn's disease: initial experience. MAGMA. 2013; 26(3):291–301. [PubMed: 23138635]
20. Dillman JR, Swanson SD, Johnson LA, et al. Comparison of noncontrast MRI magnetization transfer and T2 -Weighted signal intensity ratios for detection of bowel wall fibrosis in a Crohn's disease animal model. J Magn Reson Imaging. 2015; 42(3):801–10. [PubMed: 25504823]
21. Martens MH, Lambregts DM, Papanikolaou N, et al. Magnetization transfer ratio: a potential biomarker for the assessment of postradiation fibrosis in patients with rectal cancer. Invest Radiol. 2014; 49(1):29–34. [PubMed: 24002079]
22. Kline TL, Irazabal MV, Ebrahimi B, et al. Utilizing magnetization transfer imaging to investigate tissue remodeling in a murine model of autosomal dominant polycystic kidney disease. Magn Reson Med. 2016; 75(4):1466–73. [PubMed: 25974140]
23. Jiang K, Ferguson CM, Ebrahimi B, et al. Noninvasive Assessment of Renal Fibrosis with Magnetization Transfer MR Imaging: Validation and Evaluation in Murine Renal Artery Stenosis. Radiology. 2016:160566.
24. Lerman LO, Nath KA, Rodriguez-Porcel M, et al. Increased oxidative stress in experimental renovascular hypertension. Hypertension. 2001; 37(2 Pt 2):541–6. [PubMed: 11230332]

25. Krier JD, Ritman EL, Bajzer Z, et al. Noninvasive measurement of concurrent single-kidney perfusion, glomerular filtration, and tubular function. Am J Physiol Renal Physiol. 2001; 281(4):F630–8. [PubMed: 11553509]
26. Macfarlane, WV. Water and electrolytes in domestic animals. In: Phillis, JW., editor. Veterinary Physiology. Saunders; Philadelphia: 1976. p. 461-539.
27. Chade AR, Rodriguez-Porcel M, Grande JP, et al. Distinct renal injury in early atherosclerosis and renovascular disease. Circulation. 2002; 106(9):1165–71. [PubMed: 12196346]
28. Chade AR, Mushin OP, Zhu X, et al. Pathways of renal fibrosis and modulation of matrix turnover in experimental hypercholesterolemia. Hypertension. 2005; 46(4):772–9. [PubMed: 16172424]
29. Chade AR, Krier JD, Galili O, et al. Role of renal cortical neovascularization in experimental hypercholesterolemia. Hypertension. 2007; 50(4):729–36. [PubMed: 17635852]
30. Daghini E, Primak AN, Chade AR, et al. Assessment of renal hemodynamics and function in pigs with 64-section multidetector CT: comparison with electron-beam CT. Radiology. 2007; 243(2): 405–12. [PubMed: 17456868]
31. Huang Y, Sadowski EA, Artz NS, et al. Measurement and comparison of T1 relaxation times in native and transplanted kidney cortex and medulla. J Magn Reson Imaging. 2011; 33(5):1241–7. [PubMed: 21509885]
32. Ebrahimi B, Gloviczki M, Woollard JR, et al. Compartmental analysis of renal BOLD MRI data: introduction and validation. Invest Radiol. 2012; 47(3):175–82. [PubMed: 22183077]
33. Will S, Martirosian P, Wurslin C, Schick F. Automated segmentation and volumetric analysis of renal cortex, medulla, and pelvis based on non-contrast-enhanced T1- and T2-weighted MR images. MAGMA. 2014; 27(5):445–54. [PubMed: 24477602]
34. Daghini E, Juillard L, Haas JA, et al. Comparison of mathematic models for assessment of glomerular filtration rate with electron-beam CT in pigs. Radiology. 2007; 242(2):417–24. [PubMed: 17255413]
35. Kwon SH, Saad A, Herrmann SM, et al. Determination of Single-Kidney Glomerular Filtration Rate in Human Subjects by Using CT. Radiology. 2015; 276(2):490–8. [PubMed: 25848903]
36. Grimm PC, Nickerson P, Gough J, et al. Computerized image analysis of Sirius Red-stained renal allograft biopsies as a surrogate marker to predict long-term allograft function. J Am Soc Nephrol. 2003; 14(6):1662–8. [PubMed: 12761269]
37. Shellock FG. Radiofrequency energy-induced heating during MR procedures: a review. J Magn Reson Imaging. 2000; 12(1):30–6. [PubMed: 10931562]
38. Bernstein MA, Huston J 3rd, Ward HA. Imaging artifacts at 3.0T. J Magn Reson Imaging. 2006; 24(4):735–46. [PubMed: 16958057]
39. Dietrich O, Reiser MF, Schoenberg SO. Artifacts in 3-T MRI: physical background and reduction strategies. Eur J Radiol. 2008; 65(1):29–35. [PubMed: 18162353]
40. Textor SC, Lerman LO. Reality and renovascular disease: when does renal artery stenosis warrant revascularization? Am J Kidney Dis. 2014; 63(2):175–7. [PubMed: 24461677]
41. Eirin A, Ebrahimi B, Zhang X, et al. Changes in glomerular filtration rate after renal revascularization correlate with microvascular hemodynamics and inflammation in Swine renal artery stenosis. Circ Cardiovasc Interv. 2012; 5(5):720–8. [PubMed: 23048054]
42. Gloviczki ML, Glockner JF, Crane JA, et al. Blood oxygen level-dependent magnetic resonance imaging identifies cortical hypoxia in severe renovascular disease. Hypertension. 2011; 58(6): 1066–72. [PubMed: 22042812]
43. Gloviczki ML, Keddis MT, Garovic VD, et al. TGF expression and macrophage accumulation in atherosclerotic renal artery stenosis. Clin J Am Soc Nephrol. 2013; 8(4):546–53. [PubMed: 23258796]
44. Eirin A, Gloviczki ML, Tang H, et al. Chronic renovascular hypertension is associated with elevated levels of neutrophil gelatinase-associated lipocalin. Nephrol Dial Transplant. 2012; 27(11):4153–61. [PubMed: 22923545]
45. Eirin A, Gloviczki ML, Tang H, et al. Inflammatory and injury signals released from the post-stenotic human kidney. Eur Heart J. 2013; 34(7):540–8a. [PubMed: 22771675]
46. Eirin A, Zhu XY, Woollard JR, et al. Increased circulating inflammatory endothelial cells in blacks with essential hypertension. Hypertension. 2013; 62(3):585–91. [PubMed: 23798347]

47. Pallet N, Chauvet S, Chasse JF, et al. Urinary retinol binding protein is a marker of the extent of interstitial kidney fibrosis. PLoS One. 2014; 9(1):e84708. [PubMed: 24416268]

48. Schoenberg SO, Knopp MV, Bock M, et al. Renal artery stenosis: grading of hemodynamic changes with cine phase-contrast MR blood flow measurements. Radiology. 1997; 203(1):45–53. [PubMed: 9122415]

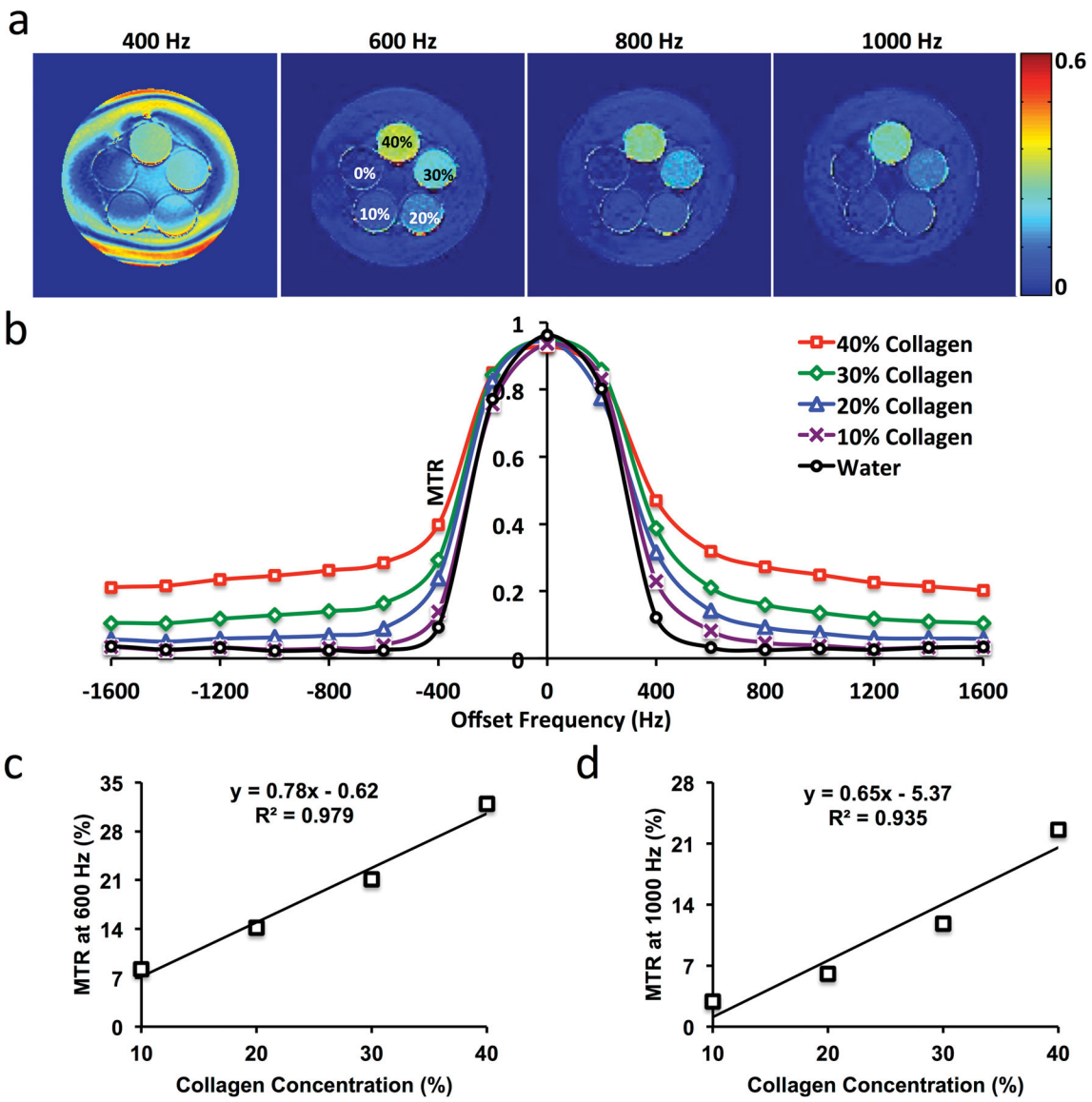

Figure 1. Collagen phantom study

(a) Magnetization transfer ratio (MTR) maps with offset-frequency at 400, 600, 800, and 1000Hz for different concentrations of collagen. **(b)** Changes in MTR with offset-frequency. (**c–d**) Linear correlation between collagen concentration and MTR at 600 (**c**) and 1000Hz (**d**).

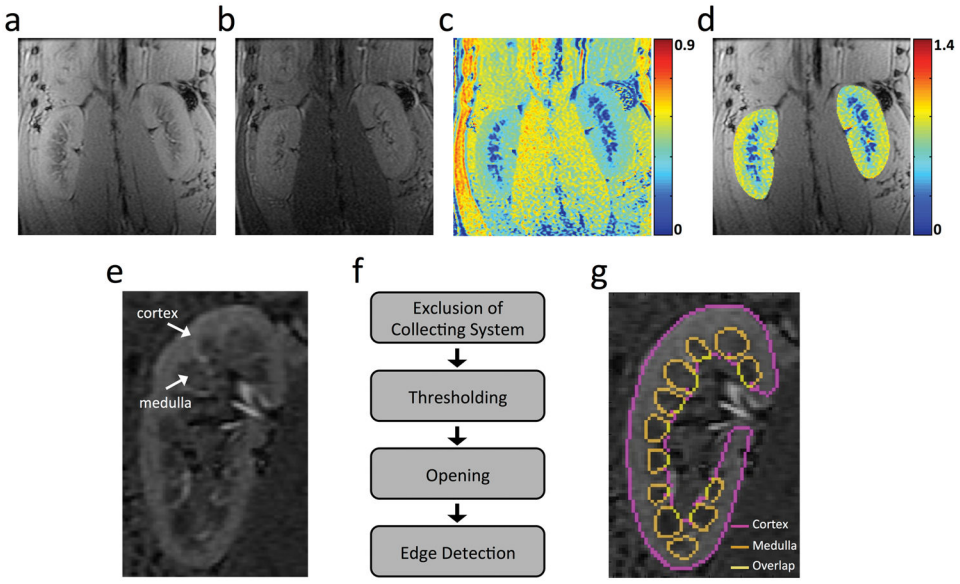

Figure 2. ***In vivo*** **MTI and kidney segmentation**

(**a–c**) Representative M_0 (**a**) and M_t (**b**) coronal images of both kidneys in a normal pig, and the MTR map (**c**) at 600Hz offset frequency. (**d**) The normalized MTR map overlaid with the M_0 image. Renal MTR was normalized by the MTR of the ipsilateral psoas muscle major to correct for B_1 variations. (**e**) A representative T_1/T_2^*-weighted image with TR/TE at 200/15.4ms shows good contrast between cortex and medulla. (**f**) Algorithm for semi-automatic selection of cortical and medullary regions of interest (ROIs). (**g**) Cortical and medullary ROIs overlaid with the T_1/T_2^*-weighted image.

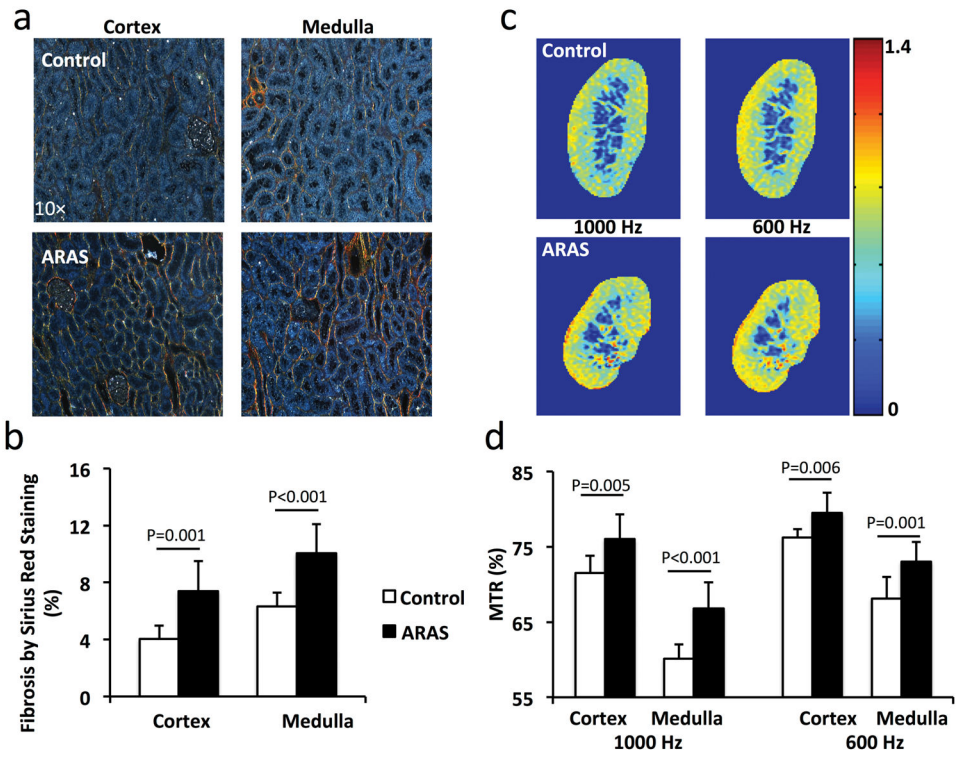

Figure 3. Renal fibrosis by Sirius red staining and MTI

a. Representative images of Sirius red-stained cortical and medullary tissues viewed under polarized light. **b.** Percentage of renal fibrosis quantified from this staining. **c**. Representative MTR maps of control and stenotic ARAS kidneys at 1000 and 600Hz. **d**. Cortical and medullary MTR. The MTR increased at both 600 and 1000Hz in ARAS kidneys.

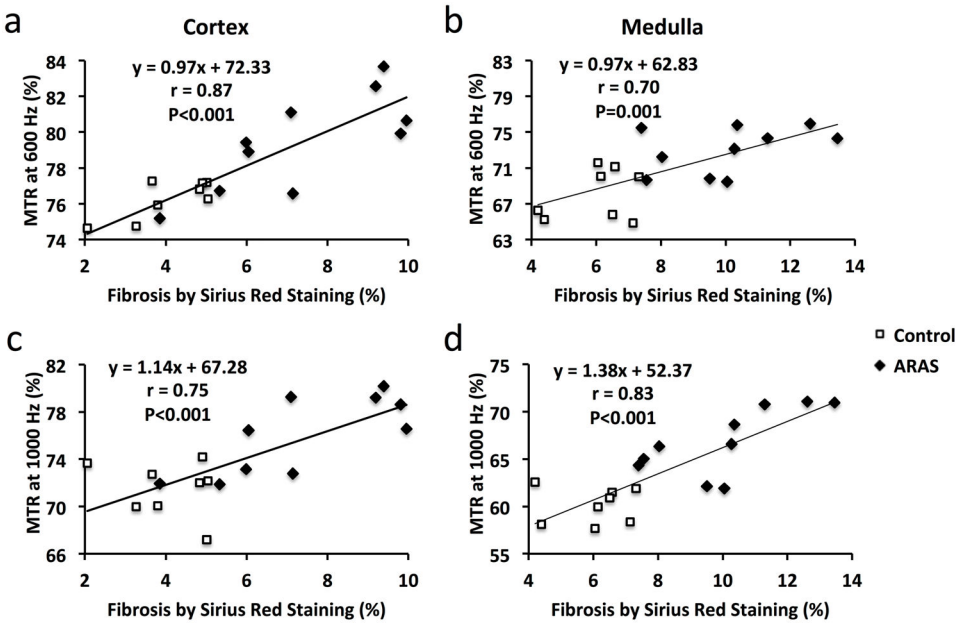

Figure 4.

Fibrosis by *ex vivo* Sirius red staining showed good correlations with *in vivo* MTR at both 600 (**a**&**b**) and 1000Hz (**c**&**d**) in ARAS both cortex and medulla.

Table 1

Characteristics and renal hemodynamics in pigs 12 weeks after ARAS or sham surgery

	Control	ARAS	P Value
Degree of Stenosis (%)	0	72.5 (30–98)	<0.001
Body Weight (kg)	54.0±6.4	62.0±5.5	0.012
MAP (mmHg)	96.7±15.0	119.7±11.7	0.005
Serum Creatinine (mg/dL)	1.55±0.14	1.88±0.17	0.003
Renal Volume (ml)			
Cortex	111.9±21.7	92.7±7.5	0.025
Medulla	20.8±3.1	14.2±2.7	<0.001
Renal Perfusion (ml/100g/min)			
Cortex	490.9±72.0	387.3±85.6	0.017
Medulla	230.1±104.1	237.2±116.4	0.894
RBF (ml/min)	687.8±128.0	452.4±96.0	0.002
GFR (ml/min)	86.8±13.6	69.1±8.7	0.010

Data are medians with ranges in parentheses or means ± standard deviations, as appropriate. ARAS=atherosclerotic renal artery stenosis; MAP=mean arterial pressure; RBF=renal blood flow; GFR=glomerular filtration rate.